14th World Congress on Computational Mechanics (WCCM)
ECCOMAS Congress 2020)
Virtual Congress: 11-–15 January 2021
F. Chinesta, R. Abgrall, O. Allix and M. Kaliske (Eds)

TOWARDS MULTIFIDELITY MODELS WITH CALIBRATION FOR TURBULENT FLOWS

SALEH REZAEIRAVESH[1,2], **RICARDO VINUESA**[1,2] **AND PHILIPP SCHLATTER**[1,2]

[1] SimEx/FLOW, KTH Engineering Mechanics, Royal Institute of Technology, Stockholm, Sweden
[2] Swedish e-Science Research Centre (SeRC), Stockholm, Sweden
salehr@kth.se, rvinuesa@mech.kth.se, pschlatt@mech.kth.se

Key words: Hierarchical Multifidelity Models, Uncertainty Quantification, Turbulent Flows, Calibration

Abstract. High-fidelity scale-resolving simulations of turbulent flows can be prohibitively expensive, especially at high Reynolds numbers. Therefore, multifidelity models (MFM) can be highly relevant for constructing predictive models for flow quantities of interest (QoIs), uncertainty quantification, and optimization. For numerical simulation of turbulence, there is a hierarchy of methodologies. On the other hand, there are calibration parameters in each of these methods which control the predictive accuracy of the resulting outputs. Compatible with these, the hierarchical MFM strategy which allows for simultaneous calibration of the model parameters as developed by Goh *et al.* [7] within a Bayesian framework is considered in the present study. The multifidelity model is applied to two cases related to wall-bounded turbulent flows. The examples are the prediction of friction at different Reynolds numbers in turbulent channel flow, and the prediction of aerodynamic coefficients for a range of angles of attack of a standard airfoil. In both cases, based on a few high-fidelity datasets, the MFM leads to accurate predictions of the QoIs as well as an estimation of uncertainty in the predictions.

1 INTRODUCTION

In science and engineering, different computational models can be derived to make realizations of the quantities of interest (QoIs) of a process or an event happening in reality. The high-fidelity (HF) models can result in highly accurate realizations, but their computational cost can also be very high. In contrast, different low-fidelity (LF) models with lower computational cost can be developed for the same process which, however, lead to lower accuracy QoIs and partial physics. On the other hand, in different applications arising in uncertainty quantification (UQ) and optimization, numerous realizations of the QoIs are required associated to the samples taken from the space of inputs/parameters in order to make reliable estimations. In this regard, multifidelity models (MFM) can be constructed by combining realizations of the HF and LF models such that a balance between the overall computational cost and predictive accuracy is achieved. In the recent years, different types of MFMs have been applied to a wide range of problems, see *e.g.* the review [20]. The use of the MFMs in studies of turbulent flows can be greatly advantageous, considering the wide range of engineering applications relying on these flows and also the high cost generally involved in the HF computations and experiments of the turbulent flows. There is a distinguishable hierarchy in the fidelity of the computational models utilized for simulation of turbulence, see *e.g.* Ref. [24]. Let us consider the wall-bounded turbulent flows where a turbulent boundary layer forms at the wall boundaries. Direct numerical simulation (DNS) can provide the highest-fidelity

results for a given turbulent flow, however it can become prohibitively expensive at high Reynolds numbers which are relevant to practical applications. The computational cost can be reduced by applying large eddy simulation (LES) which aims at directly resolving the scales larger than a defined size and modeling the unresolved effects. At the lowest cost and fidelity, Reynolds-averaged numerical simulations (RANS) of the Navier-Stokes equations can be performed which skip directly resolving any flow fluctuations. Between RANS and wall-resolving LES, other approaches such as hybrid RANS-LES and wall-modelled LES can be considered, see [24, 15]. Despite the hierarchy, there is a challenge involved in different approaches for numerical modeling of turbulence: the realizations of all fidelities are, in general, sensitive to various modeling and numerical parameters. However, the numerical effects gradually dominate the modeling parameters when shifting from RANS towards scale-resolving methods. Hereafter, such controlling parameters are referred to as tuning or calibration parameters.

Combining training data from different turbulence-simulation approaches, MFMs are constructed over the space of uncertain and design parameters/inputs. An appropriate approach to construct MFM for problems involving the simulations of turbulent flows should systematically allow for simultaneous calibration of the tuning parameters on which the realizations of different fidelities depend. An appropriate methodology which is employed in the present study is the hierarchical multifidelity predictive model proposed by Goh *et al.* [7] in which the calibration parameters of each fidelity are estimated using the data of the higher fidelity models. This model which is hereafter referred to as HC-MFM, takes into account the observation uncertainties and can be seen as an extension of the model by Higdon *et al.* [9] which was employed to fuse experimental (field) and simulation data. A fundamental component of these MFMs is the Bayesian calibration of the computer models as described in the landmark paper by Kennedy and O'Hagan [14]. At each level of the MFM, the Gaussian process regression (GPR) [21] is employed to construct surrogates or approximate expressions for the computer simulators. The application of the HC-MFM in the field of computational fluid dynamics (CFD) and turbulent flows is novel, and in this regard, the present paper aims at representing the application of the HC-MFM to two examples relevant to wall-bounded turbulent flows. The promising results and flexibility of the model make the HC-MFM a suitable choice for turbulent flows.

The HC-MFM is distinguished from the multifidelity models previously applied to the studies involving turbulent flows, which can be classified into the following three main categories: 1. The model introduced by Kennedy and O'Hagan [13] where the QoI at each fidelity is expressed as a first-order autoregressive model of the QoI at an immediately lower fidelity. Co-Kriging can be considered in this category, see *e.g.* Ref. [3] for an application in turbulence simulations. Another method which also relies on GPR is the hierarchical Kriging where the predictions of LF model assist the predictions of the high-fidelity model, see Han and Görtz [8]. 2. A class of MFM is developed based on non-intrusive polynomial chaos expansion (PCE) and stochastic collocation methods, see [17, 18]. Recently, Voet *et al.* [27] compared PCE- and Kriging-based MFMs using the data of RANS and DNS and concluded that the co-Kriging models are more accurate. 3. Multi-level multifidelity Monte Carlo (MLMF-MC) models [2] which are appropriate for the UQ forward problems. These models are developed by combining multilevel MC [5] and control-variate MC [19] methods which are developed to improve the rate of convergence of the stochastic moments of the QoIs estimated by the MC methods. Jofre *et al.* [12] applied MLMF-MC models to an irradiated particle-laden turbulent flow. The HF was considered to be DNS and the two LF models were based on a surrogate particle approach and lower resolutions for flow and particles.

The rest of the paper is organized as follow. In Section 2, a review is given to the basics of the HC-MFM

approach adopted in the present study. Section 3 is devoted to application of the MFM to an illustrative example, turbulent channel flow, and polars for an airfoil. The summary of the paper along with the conclusions and plans for future extensions is provided in Section 4.

2 HIERARCHICAL MULTIFIDELITY MODEL WITH CALIBRATION (HC-MFM)

In this section, the foundations of the hierarchical MFM with calibration (HC-MFM) developed by Goh *et al.* [7], which is used in the present study, are reviewed.

2.1 Gaussian process regression

Let $\mathbf{x} \in \mathbb{X} \subset \mathbb{R}^{d_x}$ represent the controllable inputs and parameters, adopting the notation from Ref. [14]. The design and uncertain parameters appearing in optimization and UQ analyses, respectively, can also be classified as $\mathbf{x}$. A Gaussian process (GP) $\hat{f}(\cdot)$, see *e.g.* Ref. [21], can be employed to map the inputs $\mathbf{x}$ to the outputs or QoIs of the computer codes (simulators) or field data $y \subset \mathbb{R}$, see Ref. [21]. For a finite set of samples $\{\mathbf{x}_1, \mathbf{x}_2, \ldots, \mathbf{x}_n\}$ with corresponding observations $\{y_1, y_2, \ldots, y_n\}$, the collection of $\{\hat{f}(\mathbf{x}_1), \hat{f}(\mathbf{x}_2), \ldots, \hat{f}(\mathbf{x}_n)\}$ will have a joint Gaussian (multivariate normal) distribution, [21]. The GP $\hat{f}(\mathbf{x})$ is written as:

$$\hat{f}(\mathbf{x}) \sim \mathcal{GP}\left(m(\mathbf{x}), k(\mathbf{x}, \mathbf{x}'; \boldsymbol{\beta})\right), \tag{1}$$

which is fully described by its mean $m(\mathbf{x})$ and covariance function $k(\mathbf{x}, \mathbf{x}')$ defined as:

$$m(\mathbf{x}) = \mathbb{E}[\hat{f}(\mathbf{x})], \tag{2}$$

$$k(\mathbf{x}, \mathbf{x}') = \mathbb{E}[(\hat{f}(\mathbf{x}) - m(\mathbf{x}))(\hat{f}(\mathbf{x}') - m(\mathbf{x}'))]. \tag{3}$$

In general, the GPs can be used in case of having observation noise $\boldsymbol{\varepsilon}$ in the observed data for y. Using an additive error model, we have:

$$y(\mathbf{x}) = \hat{f}(\mathbf{x}) + \boldsymbol{\varepsilon}, \tag{4}$$

where the noises are assumed to be independent and have Gaussian distributions $\boldsymbol{\varepsilon} \sim \mathcal{N}(0, \sigma^2)$. In the Gaussian process regression (GPR), given a set of training data $\mathcal{D} = \{\mathbf{x}_i, y_i\}_{i=1}^n$ the posterior and posterior predictive distributions of $\hat{f}(\cdot)$ and y, respectively, at test inputs $\mathbf{x}^* \in \mathbb{X}$ can be inferred in a Bayesian framework, see *e.g.* Ref. [21]. To this end, first a prior distribution for $\hat{f}(\mathbf{x})$, see Eq. (1), is assumed through specifying the mean and covariance functions in Eqs. (2) and (3) which depend on a set of unknown hyperparameters $\boldsymbol{\beta}$. Then, the distribution of $\boldsymbol{\beta}$ is learned using the training data. As a main advantage of the GPR, the predictions at test inputs will be accompanied by an estimate of uncertainty.

2.2 Model calibration

As pointed out in Section 1, the outputs of computational models (simulators) at a given $\mathbf{x}$ may depend on different tuning or calibration parameters, $\mathbf{t} \in \mathbb{T} \subset \mathbb{R}^{d_t}$. Given a set of observations, these parameters can be calibrated through conducting a UQ inverse problem which can be expressed in a Bayesian framework, see Kennedy and O'Hagan [14]. The calibrated model can then be employed for prediction and also for fusion of the field and simulation data, see Higdon *et al.* [9]. Consider n_1 data samples $\{(\mathbf{x}_i, y_i)\}_{i=1}^{n_1}$ observed for a physical process $\zeta(\mathbf{x})$. To statistically model the observations, a simulator $\hat{f}(\mathbf{x}, \boldsymbol{\theta})$ can be employed in which the $\boldsymbol{\theta}$ is the true value of $\mathbf{t}$ which is unknown and to be estimated from the data. In general, it is possible that even the calibrated simulator $\hat{f}(\mathbf{x}, \boldsymbol{\theta})$ produces observations which are systematically deviated from the reality. To remove such bias, a model-discrepancy term $\hat{\delta}(\mathbf{x})$ can be added to

the simulator, [14, 9]. In many applications, particularly in CFD and turbulent flow simulations, the flow solver can be run only a limited number of times. In any realization, the adopted values for the tuning parameters $\mathbf{t}$ are not necessarily optimal and hence potentially lead to outputs systematically different from the QoIs in reality. For the described calibration problem, the Kennedy and O'Hagan model [14] reads as:

$$\begin{cases} y_i = \hat{f}(\mathbf{x}_i, \boldsymbol{\theta}) + \hat{\delta}(\mathbf{x}_i) + \varepsilon_i & , \quad i = 1, 2, \cdots, n_1 \\ y_{i+n_1} = \hat{f}(\mathbf{x}_i, \mathbf{t}_i) & , \quad i = 1, 2, \cdots, n_2 \end{cases}, \tag{5}$$

where, $\hat{\cdot}$ specifies a GP and n_2 is the number of simulated data. Note that the samples $\{\mathbf{x}_i\}_{i=1}^{n_2}$ are not necessarily the same as $\{\mathbf{x}_i\}_{i=1}^{n_1}$ at which the observations are made. Given the n_1+n_2 data, the posterior distributions for the calibration parameters $\boldsymbol{\theta}$ along with those of the hyperparameters in the GPs are estimated. Further details are provided in the section below.

2.3 Hierarchical multifidelity model with calibration (HC-MFM)

Goh *et al.* [7] extended model (5) to any arbitrary number of fidelity levels which form a modeling hierarchy for the same physical process. As a main feature of the resulting MFM, each fidelity can, in general, have its own calibration parameters and also share some calibration parameters with other models. The basics of the MFM comprising three fidelity levels are explained below to the extent needed in the examples in Section 3. We assume that the fidelity of the models decreases from $M1$ to $M3$, and in practice the number of training data decreases with the model fidelity. The HC-MFM reads as [7]:

$$\begin{cases} y_{M_1}(\mathbf{x}_i) & = \hat{f}(\mathbf{x}_i, \boldsymbol{\theta}_3, \boldsymbol{\theta}_s) + \hat{g}(\mathbf{x}_i, \boldsymbol{\theta}_2, \boldsymbol{\theta}_s) + \hat{\delta}(\mathbf{x}_i) + \varepsilon_{1_i} & , \quad i = 1, 2, \cdots, n_1 \\ y_{M_2}(\mathbf{x}_{i+n_1}) & = \hat{f}(\mathbf{x}_i, \boldsymbol{\theta}_3, \mathbf{t}_{s_i}) + \hat{g}(x_i, \mathbf{t}_{2_i}, \mathbf{t}_{s_i}) + \varepsilon_{2_i} & , \quad i = 1, 2, \cdots, n_2 \\ y_{M_3}(\mathbf{x}_{i+n_1+n_2}) & = \hat{f}(\mathbf{x}_i, \mathbf{t}_{3_i}, \mathbf{t}_{s_i}) + \varepsilon_{3_i} & , \quad i = 1, 2, \cdots, n_3 \end{cases}, \tag{6}$$

where, subscript s denotes parameters shared between the models, and noises are assumed to have Gaussian distributions with zero mean. At each fidelity level, the associated simulator is created by adding a model discrepancy term to the simulator describing the immediately lower fidelity. Concatenating all training data, a vector $\mathbf{Y}$ of size $n_1+n_2+n_3$ is obtained, for which the covariance matrix can be written in terms of the covariances of $\hat{f}(\cdot)$, $\hat{g}(\cdot)$, $\hat{\delta}(\cdot)$ and observational noise:

$$\boldsymbol{\Sigma} = \boldsymbol{\Sigma}_f + \begin{bmatrix} \boldsymbol{\Sigma}_g & \mathbf{0}_{(n_1+n_2)\times n_3} \\ \mathbf{0}_{n_3\times(n_1+n_2)} & \mathbf{0}_{n_3\times n_3} \end{bmatrix} + \begin{bmatrix} \boldsymbol{\Sigma}_\delta & \mathbf{0}_{n_1\times(n_2+n_3)} \\ \mathbf{0}_{(n2+n3)\times n_1} & \mathbf{0}_{(n_2+n_3)\times(n_2+n_3)} \end{bmatrix} + \begin{bmatrix} \boldsymbol{\Sigma}_{\varepsilon_1} & \mathbf{0}_{n_1\times n_2} & \mathbf{0}_{n_1\times n_3} \\ \mathbf{0}_{n_2\times n_1} & \boldsymbol{\Sigma}_{\varepsilon_2} & \mathbf{0}_{n_2\times n_3} \\ \mathbf{0}_{n_3\times n_1} & \mathbf{0}_{n_3\times n_2} & \boldsymbol{\Sigma}_{\varepsilon_3} \end{bmatrix}. \tag{7}$$

Appropriate kernel functions should be chosen to express the structure of the covariances. Using samples i and j of the inputs and parameters, associated element in the covariance matrix $\boldsymbol{\Sigma}_f$ will be:

$$\boldsymbol{\Sigma}_{f_{ij}} = K_f(\mathbf{x}_i, \mathbf{t}_{3_i}, \mathbf{t}_{s_i}, \mathbf{x}_j, \mathbf{t}_{3_j}, \mathbf{t}_{s_j}) = \prod_{l=1}^{d_\mathbf{x}} k_{f_x}(x_{l_i}, x_{l_j}) \prod_{l=1}^{d_{\mathbf{t}_3}} k_{f_{t_3}}(t_{3_{l_i}}, t_{3_{l_j}}) \prod_{l=1}^{d_{\mathbf{t}_s}} k_{f_{t_s}}(t_{s_{l_i}}, t_{s_{l_j}}). \tag{8}$$

Similarly, expressions for $\boldsymbol{\Sigma}_{g_{ij}} = k_g(\mathbf{x}_i, \mathbf{t}_{2_i}, \mathbf{t}_{s_i}, \mathbf{x}_j, \mathbf{t}_{2_j}, \mathbf{t}_{s_j})$ and $\boldsymbol{\Sigma}_{\delta_{ij}} = K_\delta(\mathbf{x}_i, \mathbf{x}_j)$ appearing in Eq. (7) are obtained. Note that different combinations of training data for the inputs and parameters are used in each of the kernels. In all examples represented in Section 3, the exponentiated quadratic kernel function is used for $\hat{f}(\cdot)$, $\hat{g}(\cdot)$, $\hat{\delta}(\cdot)$ over the space of ξ which represents any component of $\mathbf{x}$ and $\mathbf{t}$:

$$k_f(\xi, \xi') = \lambda^{-2} \exp(-(\xi - \xi')^2/(2\ell^2)). \tag{9}$$

Therefore, hyperparameters λ and ℓ (length-scale) depend on $\hat{f}(\cdot)$, $\hat{g}(\cdot)$, $\hat{\delta}(\cdot)$ and also vary between different components of $\mathbf{x}$ and $\mathbf{t}$. The unknown parameters to estimate include calibration parameters in different models, $\boldsymbol{\theta}$, and hyperparameters $\boldsymbol{\beta}$ appearing in the kernel functions. Following the Bayes rule, the posterior distribution of these parameters reads as [7, 14, 9]:

$$\pi(\boldsymbol{\theta},\boldsymbol{\beta}|\mathbf{Y}) \propto \pi(\mathbf{Y}|\boldsymbol{\theta},\boldsymbol{\beta})\pi_0(\boldsymbol{\theta})\pi_0(\beta)\,, \tag{10}$$

where, $\pi(\mathbf{Y}|\boldsymbol{\theta},\boldsymbol{\beta})$ specifies the likelihood function and $\pi_0(\cdot)$ represents a prior distribution. In all GPs, the prior distributions for λ and ℓ in Eq. (9) are half-Cauchy and Gamma, respectively. For the noise standard-deviations, half-Cauchy priors and for the calibration parameters $\boldsymbol{\theta}$, Gaussian or uniform priors are considered. Moreover, the prior of the mean function in all GPs are considered to be constant. As a result, the predictions of the trained MFM when it is used to extrapolate in $\mathbf{x}$ (outside of the range of training samples) should be used with caution. However, according to Goh *et al.* [7] more general mean functions could, in general, be used in the MFM (6). Given the training data $\mathbf{Y}$, a Markov Chain Monte Carlo (MCMC) technique can be used to draw samples from the posterior distributions. In the present study, the described HC-MFM (6) has been implemented in `Python` using `PyMC3` [25] package with NUTS MCMC sampling [10]. The trained MFM can be used for predicting the QoI y for any new sample taken from the space of inputs $\mathbf{x}$. The predicted QoIs are ideally close to y_{M_1}. As detailed in Ref. [7], the joint distribution of the training $\mathbf{Y}$ and new y^* (associated to test sample $\mathbf{x}^*$) conditioned on $\boldsymbol{\theta},\boldsymbol{\beta}$ will have a multivariate normal distribution with a covariance matrix of the same structure as $\boldsymbol{\Sigma}$ in Eq. (7). For any joint sample drawn from the posterior distribution of $\pi(\boldsymbol{\theta},\boldsymbol{\beta}|\mathbf{Y})$, a sample prediction for y^* is made. Repeating this procedure sufficiently enough, estimations for the posterior of the predictions y^* can be achieved.

3 RESULTS AND DISCUSSION

Three examples are considered to which the HC-MFM described in the previous section is applied. The first example in Section 3.1 is used to validate the implementation of the MFM, and the next two examples are relevant to the wall-bounded turbulent flows.

3.1 An Illustrative Example

Consider the following analytical model taken from Forrester *et al.* [4] to generate high- and low-fidelity samples of the QoI y for input $x \in [0,1]$:

$$\begin{cases} y_H(x) = (\theta x - 2)^2 \sin(2\theta x - 4) \\ y_L(x) = A y_H(x) + B(x - 0.5) - C \end{cases} . \tag{11}$$

In Ref. [4], θ is taken to be fixed and equal to 6, but here it is treated as an uncertain calibration parameter that is to be estimated during the construction of the MFM. The HF training samples are taken at $x = \{0, 0.4, 0.6, 1\}$, so $n_H = 4$ is fixed. To investigate the effect of n_L, three sets of LF samples of size 10, 15, and 20 are considered which are generated by Latin hypercube sampling from the admissible space $[0,1] \times [5.8, 6.2]$ corresponding to x and t, respectively. Using the data, the HC-MFM (6) is constructed for problem (11). The first row in Figure 1 shows the predicted y with the associated 95% confidence interval (CI) along with the training data and reference true data generated with $\theta = 6$. For all n_L, the predicted y is closer to HF data than the LF data, however, for $n_L = 15$ and 20, the agreement between

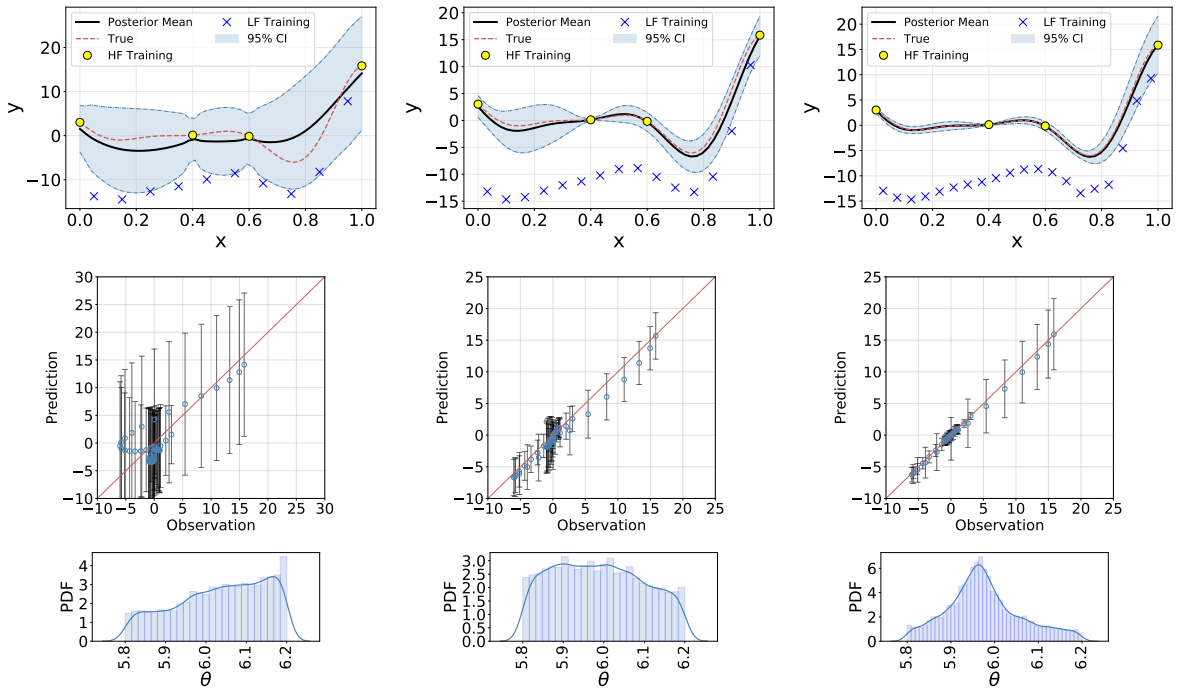

Figure 1: (Top) Predicted QoI y by HC-MFM (6) along with the training and true data, (Middle) predicted y versus true observations at 50 test samples of $x \in [0,1]$ with error bars representing 95% CI, (Bottom) posterior probability density function (PDF) of θ based on 10^4 MCMC samples. The y_H and y_L training data are generated from Eq. (11) using $A = 1$ and $B = C = 10$. The training data includes 4 HF samples combined with (left column) 10, (middle column) 15, and (right column) 20 LF samples. The true data is generated by Eq. (11) using $\theta = 6$.

the mean of the predicted y and the true data is significantly improved. A better validation can be made via the plots in the second row of Figure 1, where the predicted y and true values of y_H at 50 uniformly-spaced test samples for $x \in [0,1]$ are plotted. Clearly, increasing the number of the LF samples while keeping $n_H = 4$ fixed, improves the predictions and reduces the uncertainty. In the third row of Figure 1, the posterior densities of θ are presented. In all cases, a uniform (non-informative) prior distribution over $[5.8, 6.2]$ was considered for θ. Only for $n_L = 20$, the resulting posterior density of θ is high near the true value 6. Therefore, it is confirmed that, as explained by Goh *et al.* [7] the main capability of the HC-MFM (6) is in making accurate predictions for y and only if a sufficient number of training data is available, accurate distributions for the calibration parameters are also obtained. This is shown here by fixing n_H and increasing n_L, which is favourable in practice. It is also noteworthy that if θ was known and hence treated as a fixed parameter, then even with $n_L = 10$ very accurate predictions for y could be already achieved (not shown here).

3.2 Turbulent Channel Flow

Turbulent channel flow is one of the most canonical wall-bounded turbulent flows. The flow is developed between two parallel flat walls which are apart by a distance 2δ, and the flow is periodic in the streamwise and spanwise directions. The channel flow is fully defined by the bulk Reynolds number $\mathrm{Re}_b = U_b \delta / \nu$, where U_b and ν specify the streamwise bulk velocity and kinematic viscosity, respectively. Among dif-

ferent QoIs, here we only focus on the time-averaged friction velocity $\langle u_\tau \rangle$, which is defined as $\sqrt{\langle \tau_w \rangle / \rho}$, where τ_w and ρ are the magnitude of the wall-shear stress and fluid density, respectively. Three fidelity levels are considered: DNS (M_1), WRLES (M_2), and a reduced-order algebraic model (M_3), where the fidelity reduces from the former to the latter. We use the DNS data of Refs. [11, 16, 29]. The WRLES of channel flow have been performed at different Reynolds numbers without any explicit subgrid-scale model using OpenFOAM [28] which is an open-source finite-volume flow solver. For the details of simulations see Ref. [23], where it was shown that for a fixed resolution in the wall-normal direction, variation of the grid resolutions in the wall-parallel direction could significantly impact the accuracy of the flow QoIs. Therefore, in the context of the HC-MFM, the calibration parameters for WRLES are taken to be Δx^+ and Δz^+, which are the cell spacings in the streamwise and spanwise directions, respectively, expressed in wall-units ($\Delta x^+ = \Delta x u_\tau^\circ / \nu$ where u_τ° is the reference u_τ from DNS). At the lowest fidelity, the following reduced-order algebraic model is considered which is derived by averaging the streamwise momentum equation for the channel flow in the periodic directions and time:

$$\langle u_\tau \rangle^2 / U_b^2 = \frac{1}{\mathrm{Re}_b} \frac{\mathrm{d}}{\mathrm{d}\eta} \left((1+\zeta(\eta)) \frac{\mathrm{d}\langle u \rangle / U_b}{\mathrm{d}\eta} \right), \tag{12}$$

where η is the distance from the wall normalized by the channel half-height δ, and $\zeta(\eta)$ is the normalized eddy viscosity ν_t. Reynolds and Tiederman [22] suggested:

$$\zeta(\eta) = \frac{\nu_t(\eta)}{\nu} = \frac{1}{2} \left[1 + \frac{\kappa^2 \mathrm{Re}_\tau^2}{9} \left(1-(\eta-1)^2\right)^2 \left(1+2(\eta-1)^2\right)^2 \left(1-\exp(\frac{-\eta \mathrm{Re}_\tau}{A^+})\right)^2 \right]^{1/2} - \frac{1}{2}, \tag{13}$$

where $\mathrm{Re}_\tau = \langle u_\tau \rangle \delta / \nu$ is the friction-based Reynolds number, and κ and A^+ are two standard modeling parameters. At any Re_b (and given values of κ and A^+), Eq. (12) is integrated over $\eta \in [0,1]$ and is iteratively solved using Eq. (13) to estimate $\langle u_\tau \rangle$. Expressing the channel flow example in the terminology of MFM (6), $\langle u_\tau \rangle / U_b$ is the QoI y, $\mathbf{x} = \mathrm{Re}_b$, $\mathbf{t}_3 = (\kappa, A^+)$, and $\mathbf{t}_2 = (\Delta x^+, \Delta z^+)$. The training dataset consists of the following databases. For DNS, $\langle u_\tau \rangle$ is taken from Refs. [11, 16, 29] at $\mathrm{Re}_b = 5020$, 6962, 10000, 20000, 125000 and 200400. In total, 16 WRLES $\langle u_\tau \rangle$ samples are obtained from a design of experiment for $\Delta x^+ \sim \mathcal{U}[13,50]$ and $\Delta z^+ \sim \mathcal{U}[7,25]$ at $\mathrm{Re}_b = 5020, 6962, 10000$, and 20000. Here, we do not consider the observational uncertainty in $\langle u_\tau \rangle$ which could, for instance, be due to finite time-averaging in DNS and WRLES, but in general the HC-MFM could take such information into account. The reduced-order model (12) which is computationally cheap is run at 10 values of Re_b in range $[2000, 200200]$. At each Re_b, 9 joint samples of (κ, A^+) are generated assuming $\kappa \sim \mathcal{U}[0.36, 0.43]$ and $A^+ \sim \mathcal{U}[26.5, 29]$.

Using these training data in HC-MFM (6) and running the MCMC samples for 5000 samples, after an extra 2000 samples discarded due to burn-in, the model is constructed. According to Figure 2(a), the predicted mean of $\langle u_\tau \rangle / U_b$ follows the trend of the DNS data. This approximately holds even at high Reynolds numbers, where there is a large systematic error in the algebraic model and no WRLES data is available. As expected, in this range due to scarcity of the DNS data over a wide range of Re_b the uncertainty in the predictions is high. The plot in Figure 2(b) shows the joint MCMC samples of the calibration parameters κ, A^+, Δx^+, and Δz^+ along with the histogram of each parameter. The prior distribution for κ and A^+ were assumed to be uniform over ranges $[0.36, 0.43]$ and $[26.5, 29]$, respectively. The priors for Δx^+ and Δz^+ were taken to be Gaussian with the mean set at the associated lowest training

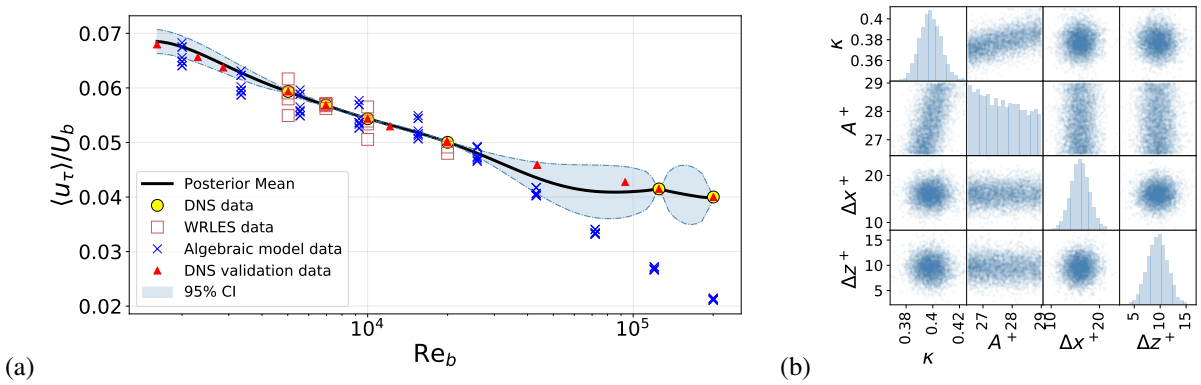

Figure 2: (a) Mean prediction of $\langle u_\tau \rangle / U_b$ and associated 95% CI along with the training data and validation data from DNS of Refs. [11, 16, 29], (b) posterior distribution and MCMC samples of parameters κ, A^+, Δx^+, and Δz^+.

sample value. The resulting posterior densities of κ and A^+ are not uniform and the samples of these two parameters are correlated. In contrast, for Δx^+ and Δz^+ the posterior densities are still close to Gaussian and no correlation between the samples is observed.

3.3 Polars For the NACA0015 Airfoil

In this section, the HC-MFM model (6) is applied to a set of data for lift and drag coefficients, C_L and C_D, of a wing with a NACA0015 airfoil profile at Reynolds number 1.6×10^6. The flow angle of attack (AoA) is the design parameter $\mathbf{x}$. The data comprises of the followings: wind-tunnel experiments by Bertagnolio [1] (M_1), detached-eddy simulations (DES) ($M2$) and two-dimensional RANS (M_3) both by Gilling *et al.* [6]. In their numerical study, Gilling *et al.* [6] investigated the sensitivity of the DES results with respect to the resolved turbulence intensity (TI) of the fluctuations imposed at the inlet boundary. The sensitivity was found to be particularly significant near the stall. Therefore, when constructing an MFM, the calibration parameter t_2 in fidelity M_2 is taken to be the TI. The admissible range of $\mathbf{x} = \text{AoA}$ is $[0^\circ, 20^\circ]$, over which the experimental and RANS data are available, see Refs. [1, 6]. The training HF data are taken to be a subset of size 7 from the experimental data of Ref. [1]. The rest of the experimental data are used to validate the predictions of the MFM model. For the purpose of examining the capability of the MFM in a more challenging situation, the training HF samples are intuitively selected to exclude the AoAs near the stall. The DES data of Gilling *et al.* [6] are available at 6 AoA $\in [8^\circ, 19^\circ]$ and 5 different values of TI. Employing these training data in the HC-MFM (6) and drawing 10^4 MCMC samples after excluding extra 5000 initial samples for burn-in, the predictions for C_L and C_D shown in Figure 3(a,c) are obtained. The expected value of the predictions has a trend similar to that of the experimental validation data of Ref. [1] and is not diverted towards the physically-invalid RANS data at AoA $\gtrsim 10^\circ$. A more elaborate comparison is made through plotting the MFM predictions against the validation data in Figure 3(b,d). For both C_L and C_D, the agreement between the predicted mean values with validation data at lower AoAs (before stall) is excellent and for most of the higher AoAs, even near and after the stall, is fairly good. Due to the scarcity of the HF training data, the error bars at the predicted values can be relatively large, as more evident in the case of C_D in Figure 3(d).

When training the HC-MFM (6), the TI in DES as the only calibration parameter in M_2, as well as the hyperparameters in all the GPs are estimated. To make the model capable of including the impact of the

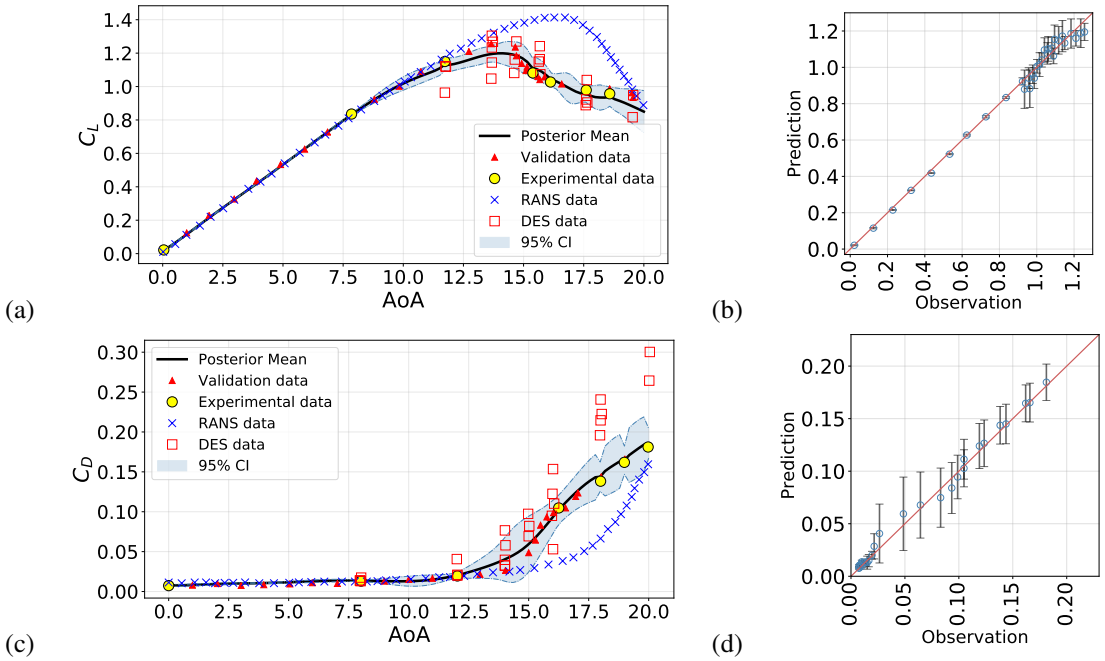

Figure 3: (a) Lift coefficient C_L and (c) drag coefficient C_D plotted against the angle of attack: the HC-MFM (6) is trained by the experimental data of Ref. [1] (yellow circles), as well as the DES (squares) and RANS (crosses) data by Gilling *et al.* [6]. The DES are performed in Ref. [6] with the resolved turbulence intensities TI $= 0\%, 0.1\%, 0.5\%, 1\%$, and 2% at the inlet. The validation data (red triangles) are also taken from the experiments of Ref. [1]. The mean prediction by the HC-MFM (6) is represented by the solid line along with associated 95% confidence interval. (b) C_L, (d) C_D predictions by HC-MFM plotted against the validation data. The error bars represent the 95% CI.

stall, we need to introduce the stall AoA as a new parameter x_{stall} in the model discrepancy term $\hat{\delta}(\mathbf{x})$ in Eq. (6). Accordingly, the associated kernel function Σ_δ appearing in Eq. (3) is modified as:

$$\Sigma_{\delta_{ij}} = K_{\delta_1}(\mathbf{x}_i, \mathbf{x}_j; x_{\text{stall}}) + K_{\delta_2}(\mathbf{x}_i, \mathbf{x}_j; x_{\text{stall}}), \tag{14}$$

where, $k_{\delta_1}(\cdot,\cdot)$ and $k_{\delta_2}(\cdot,\cdot)$ refer to the kernel functions before and after the stall, respectively. These kernels are taken to be of the exponentiated quadratic form, see Eq. (9), with own specific hyperparameters. Another hyperparameter is also introduced to smoothly merge the above two kernels at x_{stall}. Figure 4 shows the posterior densities of different parameters appearing in the MFM constructed for C_L and C_D. As expected, the distribution of the kernels' hyperparameters varies between the two QoIs. But more importantly, the posterior distributions of x_{stall} and calibrated TI are also dependent on the QoI. This clearly shows the suitability of the present class of MFMs in which calibration of the parameters of different fidelities is performed as a part of constructing the MFM. The alternative strategy, which is common in practice but seems to be inefficient (given the present observations), would be to calibrate the LF models by HF data of a QoI and then run the calibrated LF model to make realizations of all QoIs.

As a general goal, MFM constructs a surrogate for the QoIs in the space of the design/controlled parameters in a way that the surrogate outputs are close to the HF data. In this regard, the MFMs facilitate applying different types of sample-based UQ techniques and optimization, see *e.g.* [26]. In connection to

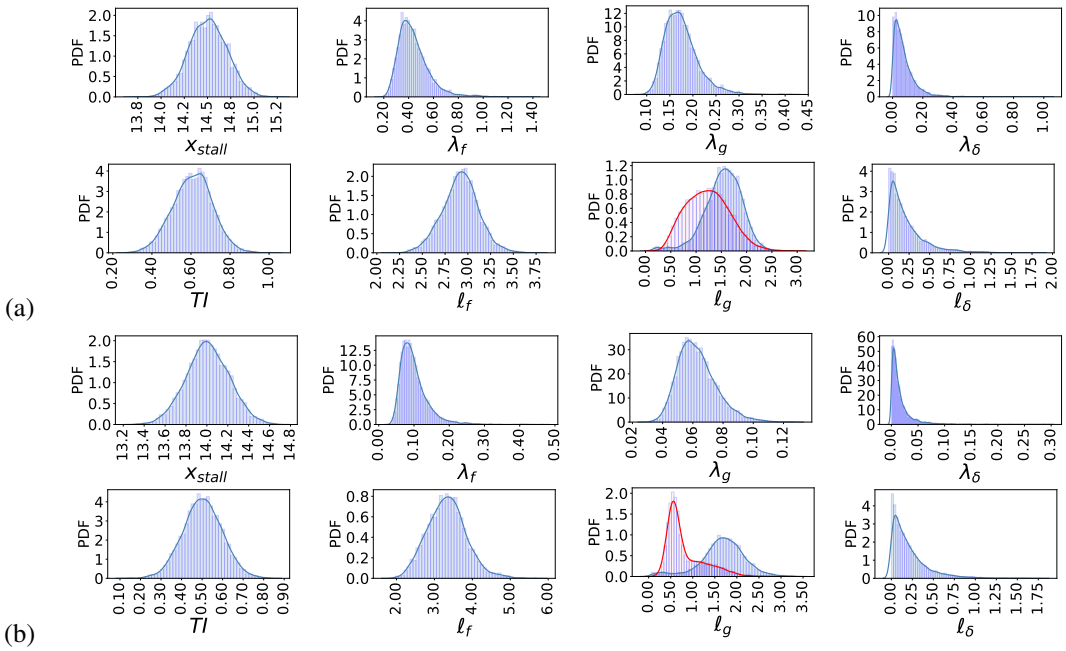

Figure 4: Posterior PDFs of the calibration parameters and hyperparameters of the GPs appearing in the HC-MFM (6) for (a) C_L and (b) C_D. Associated training data and predictions are shown in Figure 3. In the plots of ℓ_g, the blue and red histograms are corresponding to AoA and TI, respectively.

the present example, consider a UQ forward problem to estimate the statistical moments of C_L and C_D due to the uncertainty in the AoA. For instance, assume AoA $\sim \mathcal{U}[15^\circ, 17^\circ]$. Then, the estimated expectation and variance of C_L and C_D with associated 95% CI are: $\mathbb{E}_{\mathbf{x}}[C_L] = 1.0636 \pm 0.0474$, $\mathbb{V}_{\mathbf{x}}[C_L] = 3.1261 \times 10^{-3} \pm 3.3658 \times 10^{-3}$, $\mathbb{E}_{\mathbf{x}}[C_D] = 0.09413 \pm 0.01958$, and $\mathbb{V}_{\mathbf{x}}[C_D] = 4.3988 \times 10^{-4} \pm 5.8921 \times 10^{-4}$. Note that without the HC-MFM model, and only based on the data of RANS or/and DES, such estimations would be inaccurate.

4 SUMMARY AND CONCLUSIONS

The hierarchical multifidelity model with calibration (HC-MFM) developed by Goh *et al.* [7] is applied to three examples including two relevant ones to turbulent flows. The HC-MFM can be constructed for arbitrary number of fidelity levels and is well-suited to the simulation of turbulent flows since as a part of the MFM construction the influential parameters at each fidelity can be calibrated. This is an important feature noting that in all approaches for simulating turbulence, different numerical, modeling and uncertain parameters can influence the QoIs. Given that Gaussian processes are used in HC-MFM, the possibility of incorporating observational uncertainties at all fidelity levels is also provided. Based on the examples, two main conclusions are drawn. First, for a fixed number of high-fidelity data the HC-MFM prioritizes the prediction of QoIs so that they become as close as possible to the high-fidelity data, while the posterior distributions of the calibrated parameters are found to be accurate only if sufficiently many low-fidelity data are provided. A similar conclusion was drawn by Goh *et al.* [7] by systematically increasing the amount of both high- and low-fidelity data. It is also concluded that for the data obtained from the same set of realizations, the posterior distributions of the calibration parameters depend on the

QoIs. In other words, the calibration parameters are more numerical than physical and hence, predictions by HC-MFM can be more accurate than the case of a-priori calibrating the low-fidelity models by high-fidelity data of one particular QoI. The present study may be extended in several directions. In addition to scalar QoIs, spatio–temporal fields can be considered in the HC-MFM. The observation uncertainty in the data, for instance due to numerics and sampling errors, can be taken into account, as well. The use of the HC-MFM in a UQ forward problem or optimization based on a large-dimensional parameter space will be considered in the future.

Acknowledgements

This work has been supported by the EXCELLERAT project, which has received funding from the European Union's Horizon 2020 research and innovation programme under grant agreement No 823691. Additional funding was provided by the Knut and Alice Wallenberg Foundation (KAW).

REFERENCES

[1] F. Bertagnolio. *NACA0015 Measurements in LM Wind Tunnel and Turbulence Generated Noise*. Number 1657(EN) in Denmark. Forskningscenter Risoe. Danmarks Tekniske Universitet, 2008.

[2] H. R. Fairbanks, A. Doostan, C. Ketelsen, and G. Iaccarino. A low-rank control variate for multilevel Monte Carlo simulation of high-dimensional uncertain systems. *J. Comput. Phys*, 341:121–139, 2017.

[3] J. Fatou Gomez. *Multi-fidelity Co-Kriging Optimization using Hybrid Injected RANS and LES*. PhD thesis, Delft University of Technology, 2018.

[4] A. I. Forrester, A. Sóbester, and A. J. Keane. Multi-fidelity optimization via surrogate modelling. *Proceedings of the Royal Society A*, 463(2088):3251–3269, 2007.

[5] M. B. Giles. Multilevel Monte Carlo path simulation. *Operations Research*, 56(3):607–617, 2008.

[6] L. Gilling, N. Sørensen, and L. Davidson. Detached eddy simulations of an airfoil in turbulent inflow. *47th AIAA Aerospace Sciences Meeting*, 24(AIAA 2009-270):1–13, 2009.

[7] J. Goh, D. Bingham, J. P. Holloway, M. J. Grosskopf, C. C. Kuranz, and E. Rutter. Prediction and computer model calibration using outputs from multifidelity simulators. *Technometrics*, 55(4):501–512, 2013.

[8] Z.-H. Han and S. Görtz. Hierarchical kriging model for variable-fidelity surrogate modeling. *AIAA Journal*, 50(9):1885–1896, 2012.

[9] D. Higdon, M. Kennedy, J. C. Cavendish, J. A. Cafeo, and R. D. Ryne. Combining field data and computer simulations for calibration and prediction. *SIAM J. Sci. Comput.*, 26(2):448–466, 2004.

[10] M. D. Hoffman and A. Gelman. The No-U-Turn Sampler: Adaptively setting path lengths in Hamiltonian Monte Carlo. *Journal of Machine Learning Research*, 15(47):1593–1623, 2014.

[11] K. Iwamoto, Y. Suzuki, and N. Kasagi. Reynolds number effect on wall turbulence: toward effective feedback control. *International Journal of Heat and Fluid Flow*, 23(5):678–689, 2002.

[12] L. Jofre, G. Geraci, H. R. Fairbanks, A. Doostan, and G. Iaccarino. Exploiting multi-fidelity strategies to quantify uncertainty in irradiated particle-laden turbulent flow. *Proceedings of the 7th Eu-*

ropean Conference on Computational Fluid Dynamics, pages 1–12, 2018.

[13] M. C. Kennedy and A. O'Hagan. Predicting the output from a complex computer code when fast approximations are available. *Biometrika*, 87(1):1–13, 2000.

[14] M. C. Kennedy and A. O'Hagan. Bayesian calibration of computer models. *Journal of the Royal Statistical Society: Series B (Statistical Methodology)*, 63(3):425–464, 2001.

[15] J. Larsson, S. Kawai, J. Bodart, and I. Bermejo-Moreno. Large eddy simulation with modeled wall-stress: recent progress and future directions. *Bulletin of the JSME*, 3(1), 2016.

[16] M. Lee and R. D. Moser. Direct numerical simulation of turbulent channel flow up to $Re_\tau \approx 5200$. *J. Fluid Mech.*, 774:395–415, 2015.

[17] L. W.-T. Ng and M. Eldred. Multifidelity uncertainty quantification using non-intrusive polynomial chaos and stochastic collocation. *53rd AIAA/ASME/ASCE/AHS/ASC Structures, Structural Dynamics and Materials Conference*, (AIAA 2012-1852):1–17, 2012.

[18] P. S. Palar, T. Tsuchiya, and G. T. Parks. Multi-fidelity non-intrusive polynomial chaos based on regression. *Computer Methods in Applied Mechanics and Engineering*, 305:579 – 606, 2016.

[19] R. Pasupathy, B. W. Schmeiser, M. R. Taaffe, and J. Wang. Control-variate estimation using estimated control means. *IIE Transactions*, 44(5):381–385, 2012.

[20] B. Peherstorfer, K. Willcox, and M. Gunzburger. Survey of multifidelity methods in uncertainty propagation, inference, and optimization. *SIAM Review*, 60(3):550–591, 2018.

[21] C. E. Rasmussen and C. K. I. Williams. *Gaussian Processes for Machine Learning (Adaptive Computation and Machine Learning)*. The MIT Press, 2005.

[22] W. C. Reynolds and G. W. M. F. Tiederman. Stability of turbulent channel flow, with application to Malkus's theory. *J. Fluid Mech.*, 27(part 2):253–272, 1967.

[23] S. Rezaeiravesh and M. Liefvendahl. Effect of grid resolution on large eddy simulation of wall-bounded turbulence. *Physics of Fluids*, 30(5):055106, 2018.

[24] P. Sagaut, S. Deck, and M. Terracol. *Multiscale and Multiresolution Approaches in Turbulence*. Imperial College Press, 2nd edition, 2013.

[25] J. Salvatier, T. V. Wiecki, and C. Fonnesbeck. Probabilistic programming in Python using PyMC3. *PeerJ Computer Science*, 2:e55, 2016.

[26] R. C. Smith. *Uncertainty Quantification: Theory, Implementation, and Applications*. Society for Industrial and Applied Mathematics, Philadelphia, PA, USA, 2013.

[27] L. J. Voet, R. Ahlfeld, A. Gaymann, S. Laizet, and F. Montomoli. A hybrid approach combining DNS and RANS simulations to quantify uncertainties in turbulence modelling. *Applied Mathematical Modelling*, 89:885 – 906, 2021.

[28] H. Weller, G. Tabor, H. Jasak, and C. Fureby. A tensorial approach to computational continuum mechanics using object-oriented techniques. *Computers in Physics*, 12(6):620–631, 1998.

[29] Y. Yamamoto and Y. Tsuji. Numerical evidence of logarithmic regions in channel flow at $\mathrm{Re}_\tau = 8000$. *Phys. Rev. Fluids*, 3:012602, 2018.